

Novel weak-ferromagnetic metallic state in heavily doped $\text{Ba}_{1-x}\text{K}_x\text{Mn}_2\text{As}_2$

Jin-Ke Bao,¹ Hao Jiang,¹ Yun-Lei Sun,¹ Wen-He Jiao,¹ Chen-Yi Shen,¹ Han-Jie Guo,¹
Ye Chen,¹ Chun-Mu Feng,¹ Hui-Qiu Yuan,¹ Zhu-An Xu,¹ Guang-Han Cao,^{1,2,*}
Ryo Sasaki,² Toshiaki Tanaka,² Kazuyuki Matsubayashi,² and Yoshiya Uwatoko²

¹Department of Physics, Zhejiang University, Hangzhou 310027, China

²Institute for Solid State Physics, The University of Tokyo, Kashiwanoha, Kashiwa, Chiba 277-8581, Japan

Heavily doped $\text{Ba}_{1-x}\text{K}_x\text{Mn}_2\text{As}_2$ ($x=0.19$ and 0.26) single crystals were successfully grown, and investigated by the measurements of resistivity and anisotropic magnetization. In contrast to the antiferromagnetic insulating ground state of the undoped BaMn_2As_2 , the K-doped crystals show metallic conduction with weak ferromagnetism below ~ 50 K and Curie-Weiss-like in-plane magnetic susceptibility above ~ 50 K. Under high pressures up to 6 GPa, the low-temperature metallicity changes into a state characterized by a Kondo-like resistivity minimum. Electronic structure calculations for $x=0.25$ using $2 \times 2 \times 1$ supercell reproduce the hole-doped metallic state. The density of states at Fermi energy have significant As $4p$ components, suggesting that the $4p$ holes are mainly responsible for the metallic conduction. Our results suggest that the interplay between itinerant $4p$ holes and local $3d$ moments are mostly responsible for the novel metallic state.

PACS numbers: 71.30.+h; 75.30.-m; 72.80.Ga; 71.20.Ps

I. INTRODUCTION

The discovery of Fe-based pnictide superconductors^{1,2} has also brought considerable research interest on the isostructural pnictides containing other transition metals, like LaT_MAsO and $\text{BaT}_{M2}\text{As}_2$ (T_M stands for $3d$ transition metals such as Mn, Fe, Co and Ni). Among them, the Mn-based materials are particularly worthy of investigation, because they exhibit antiferromagnetic (AFM) *insulating* ground state, similar to the parent compounds of high- T_c cuprates and colossal magnetoresistance manganites. According to the paradigm of metal-insulator transition,³ it is expected to realize an insulator-to-metal transition either by charge carrier doping (band filling control) or by applying high pressures (band-width control) in the Mn-based pnictides. Very recently Tokura and co-workers⁴ indeed observed this kind of transition via electron doping in oxygen-deficient $\text{SmMnAsO}_{1-\delta}$. Coincidentally we realized the metallization by hole doping in $\text{La}_{1-x}\text{Sr}_x\text{MnAsO}$.⁵ Notably the metallic $\text{La}_{0.9}\text{Sr}_{0.1}\text{MnAsO}$ polycrystalline sample showed an unusually large Seebeck coefficient of $\sim 240\mu\text{V}/\text{K}$.

Although the $\text{BaT}_{M2}\text{As}_2$ family all crystallize in elongated ThCr_2Si_2 -type structure, they show diverse physical properties. BaFe_2As_2 is a striped AFM semimetal with an ordered moment of $\sim 0.9\mu_B/\text{Fe}$,⁶ serving as a prototype parent compound of Fe-based superconductors.⁷ $\text{Ba}_2\text{Cr}_2\text{As}_2$ was found to be a G -type AFM metal with an ordered moment of $\sim 2\mu_B/\text{Cr}$ and with strong Cr $3d$ -As $4p$ hybridization.⁸ BaCo_2As_2 exhibits a renormalized paramagnetic metal in proximity to a possible ferromagnetic quantum critical point.⁹ BaNi_2As_2 was demonstrated as a fully-gapped superconductor.¹⁰ It seems that the count of $3d$ electrons determines the physical properties, and the metallic states can be understood by the partial filling of $3d$ electrons. Exceptionally BaMn_2As_2 has a G -type AFM *insulating* ground state with a large

moment ($\sim 3.9\mu_B/\text{Mn}$) and a high Néel temperature (~ 620 K).¹¹⁻¹⁴ The magnetic properties can be well described by the $J_1 - J_2 - J_c$ Heisenberg exchange model.¹⁵

The unique insulating property of BaMn_2As_2 makes it promising to explore novel states of matter via applying high pressures as well as various chemical doping just like those^{7,16-19} employed in BaFe_2As_2 . Some doping studies^{20,21} were recently performed in BaMn_2As_2 system. For the Mn-site doping,²⁰ unfortunately, many transition metals do not substitute for Mn at levels above 0.5%. Although Cr and Fe (Mn's neighbors in the Periodic Table) can substitute for Mn significantly (at levels of 4.4% and 10%, respectively), these substitutions hardly change the electronic transport and magnetic properties. Very recently Pandey et al.²¹ succeeded in doping small amount of K (1.6% in single crystals and 5% in polycrystals) into BaMn_2As_2 . They demonstrated that the K doping induced hole carriers, and changed the system into a metallic state. Interestingly the local moment of Mn as well as the Néel temperature is basically preserved against the K doping. It was thus advocated that the new class of materials bridged the gap between the iron pnictide and cuprate high T_c materials.²¹ Another recent study²² showed a pressure-induced metallization in BaMn_2As_2 .

Motivated by the hole-doping result in LaMnAsO ,⁵ we also succeeded in growing K-doped BaMn_2As_2 single crystals.²³ In this paper, we report the measurements of electrical resistivity, magnetoresistivity, anisotropic magnetization and heat capacity for the single crystals of heavily doped $\text{Ba}_{1-x}\text{K}_x\text{Mn}_2\text{As}_2$ (BKMA) with $x=0.19$ and 0.26 . The samples show metallic behavior with the resistivity one order of magnitude smaller than previously reported²¹ in the lightly K-doped samples. Besides, a weak ferromagnetic transition was observed below ~ 50 K on the background of local-moment AFM order. Novel metallic state is also manifested by the Curie-Weiss-like in-plane magnetic susceptibility, and the appearance of a

minimum in low temperature resistivity under high pressures. Electronic structure calculations suggest that the interplay between itinerant As $4p$ holes and local Mn $3d$ moments plays an important role for the strange metallicity in BKMA system.

II. EXPERIMENTAL

Single crystals of BKMA were grown by high-temperature spontaneous nucleations using MnAs as the self flux. First, MnAs was prepared by reacting stoichiometric mixture of Mn and As powder at 1073 K for 16 hours in an evacuated quartz tube. Second, Ba and K pieces with the presynthesized MnAs powder were put into an alumina crucible in the molar ratios of $(\text{Ba}+\text{K}):\text{MnAs}=1:5$, and $\text{K}:\text{Ba}=0$ and 1. All the starting materials have the purity $\geq 99.9\%$. For the growth of K-doped crystals, the alumina crucible was placed into an iron tube sealed by an iron cap, in order to protect the potassium from reacting with quartz tube. All the procedures were conducted in a glove box filled argon with the water and oxygen content below 0.1 ppm. The iron tube was slowly heated up to 1503 K holding for 8 hours in a furnace filled with protective argon atmosphere. Then it was allowed to cool down to 1323 K at a cooling rate of 5 K/h, followed by shutting off the furnace. Shiny black crystals with typical size of $2\text{mm} \times 2\text{mm} \times 0.1\text{mm}$ were obtained. The as-grown crystals were found to have two categories of K content. Those with higher K content ($x=0.33\sim 0.43$) was inhomogeneous (e.g., they showed broad x-ray diffraction and multiple weak ferromagnetic transitions), so we will not discuss them in this paper. Others with lower K content ($x=0.15\sim 0.27$) had homogeneous distribution of K. The two crystals studied here were from the second category, and they were carefully cleaved and selected to remove the flux MnAs as far as possible. Note that the crystals had been stored in a glove box free of oxygen and water at room temperature for 5 months.

X-ray diffraction was performed at room temperature using a D/Max-rA diffractometer with Cu K_α radiation and a graphite monochromator. As usual, the crystallographic c axis was found to be perpendicular to the crystal plate. Therefore, the lattice parameter c was able to be calculated by the $(00l)$ multiple diffractions after making the zero shift correction. The content of the doped potassium in the single crystals were measured by energy-dispersive x-ray spectroscopy (EDS), equipped in a field-emission scanning electron microscope. The electrical resistivity was measured by a standard four-probe method. Gold wires were carefully attached to the crystal by using silver paint under an optical microscope. The error caused by the size of the electrodes leads to the total uncertainty in the absolute resistivity of 10%. Hydrostatic pressure was generated by a cubic anvil cell immersed in a cryostat.²⁴ The magnetic property was measured on a commercial Quantum Design magnetic

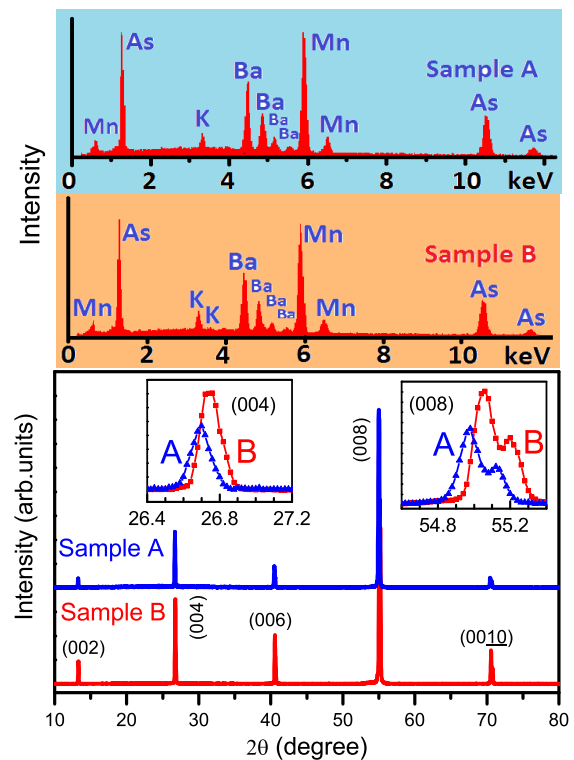


FIG. 1: (Color online) Compositional and structural characterizations of the two $\text{Ba}_{1-x}\text{K}_x\text{Mn}_2\text{As}_2$ single crystals. The upper panels are the typical energy-dispersive x-ray spectra which give $x=0.19(1)$ and $0.26(1)$ for samples A and B, respectively. The lower panel shows the x-ray diffraction patterns of the identical samples. The magnified (004) and (008) reflections are displayed in the insets.

property measurement system (MPMS-5). The magnetization was measured under $\mu_0 H=1$ T in the zero-field cooling mode.

The electronic structure calculations were based on density functional theory, using the CASTEP module of Materials Studio.²⁵ The calculations employed ultrasoft pseudopotentials and a plane-wave expansion for the wave functions. The exchange correlation effects were treated by the generalized gradient approximation with the Perdew-Burke-Ernzerhof functional. The plane-wave basis energy cutoff was set at 330 eV. For the calculation of 25% K-doped BaMn_2As_2 , a $2 \times 2 \times 1$ supercell was built. From the experimental result, G -type AFM order was assumed to be the ground state. For bandstructure and density-of-states (DOS) calculations, $26 \times 26 \times 15$ and $5 \times 5 \times 3$ k -points were used, respectively.

III. RESULTS AND DISCUSSION

A. Sample Characterizations

The BKMA single crystals were characterized by XRD and EDS experiments. The typical EDS patterns for the

samples studied here, shown in the upper panels of Fig. 1, indicate the presence of only four elements K, Ba, Mn and As. The quantitative analysis gives the chemical formula as $\text{Ba}_{0.81(3)}\text{K}_{0.19(1)}\text{Mn}_2\text{As}_2$ and $\text{Ba}_{0.74(3)}\text{K}_{0.26(1)}\text{Mn}_2\text{As}_2$ for Sample A (\$A) and Sample B (\$B), respectively. The XRD patterns were recorded for the plate-like crystals placed horizontally on a sample holder. The diffraction peaks are very sharp [with the full width at half maximum (FWHM) about 0.1°], indicating good homogeneity and crystallinity. They were indexed as $(00l)$ reflections with $l=\text{even}$, consistent with the body-centered tetragonal structure (space group: $I4/mmm$). The crystallographic c axes (13.350\AA for \$A and 13.330\AA for \$B) are 0.77% and 0.92% smaller than that of the undoped BaMn_2As_2 (13.454\AA). This phenomenon is in contrast with the $\text{Ba}_{1-x}\text{K}_x\text{Fe}_2\text{As}_2$ system, which shows remarkable *increase* in c with the K doping.⁷ The possible reason is the strong $p-d$ hybridizations in BaMn_2As_2 ,¹⁴ resulting in the shortening of Mn–As bondlength (and thus shrinkage of c axes) when doping holes in the $p-d$ valence bands.

B. Resistivity

Figure 2 shows the temperature dependence of electrical resistivity [$\rho(T)$] of the undoped BaMn_2As_2 as well as the BKMA crystals. The $\rho(T)$ data of the parent material indicate semiconducting behavior with room-temperature resistivity of $430\text{ m}\Omega\cdot\text{cm}$. However, the temperature coefficient is positive (metallic-like) for $T > 190\text{ K}$. This result is qualitatively consistent with those in previous reports.^{12,14} The absolute values of the resistivity are closer to those in Ref.¹⁴. The data of $60\text{ K} < T < 90\text{ K}$ can be well fitted with the standard thermally-activated equation, i.e., $\rho \propto \exp(E_a/k_B T)$. The fitted result gives the activation energy $E_a=0.027\text{ eV}$, precisely coinciding with the previous report.¹² This suggests that the bandgap E_g is no less than $2E_a=0.054\text{ eV}$, which agrees with the previous band calculation result ($E_g \sim 0.1\text{ eV}$).¹⁴ We note that the $\rho(T)$ data in the high-temperature regime obey the non-adiabatic small-polaron transport behavior, i.e., $\rho \propto T^{3/2}\exp(\Delta/k_B T)$. The fitted Δ value is 0.040 eV (using the $\rho(T)$ data from 60 K to 160 K). Note that $\Delta=E_a + E_{hop}$, therefore, the polaron-hopping potential E_{hop} is estimated to be 0.013 eV . This small-polaron transport behavior suggests that the dominant activated charge carriers are weakly localized instead of being itinerant in the parent compound. It is noted that neither thermally-activated model nor small-polaron one accounts for the low-temperature ($T < 60\text{ K}$) data well. Instead the electrical transport tends to be dominated by variable range hopping (VRH) in the low-temperature regime, because the $\rho(T)$ data better fit the Mott's law of three-dimensional VRH,²⁶ i.e., $\rho \propto \exp(T_0/T)^{1/4}$.

In contrast to the semiconducting behavior above for undoped BaMn_2As_2 crystals, the K-doped crystals show

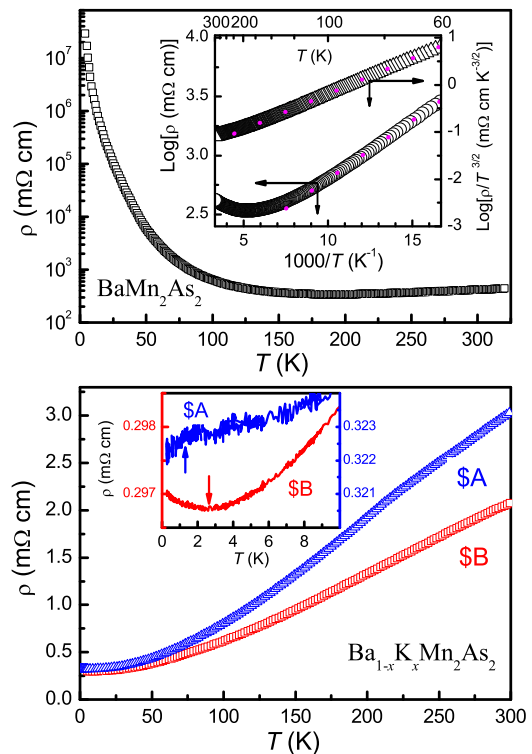


FIG. 2: (Color online) Temperature dependence of resistivity for BaMn_2As_2 (upper panel) and $\text{Ba}_{1-x}\text{K}_x\text{Mn}_2\text{As}_2$ (lower panel) crystals. The upper inset plots $\log\rho$ and $\log(\rho/T^{3/2})$ against the reciprocal of temperature, corresponding to thermally-activated model and non-adiabatic small-polaron transport model, respectively. The lower inset shows the low-temperature resistivity. The K content of \$A and \$B is 0.19(1) and 0.26(1), respectively.

metallic conduction in the whole temperature range, as shown in the lower panel of Fig. 2. The room-temperature resistivity is $2\sim 3\text{ m}\Omega\cdot\text{cm}$, which is over two orders of magnitude smaller than that of BaMn_2As_2 , and about one order of magnitude smaller than that reported for the lightly K-doped samples with $x=0.016$ and 0.05 .²¹ This further confirms insulator-to-metal transition in BKMA. Below 1.5 K , \$A with $x=0.19$ shows a tiny drop in resistivity. However, the resistivity of \$B ($x=0.26$) exhibits an upturn below 2.8 K , like the well-known Kondo effect.

We chose the $x=0.19$ sample to study its pressure effect. Under high pressures, while the high-temperature resistivity decreases rapidly, the low-temperature resistivity decreases subtly. By careful examination, the low-temperature metallicity changes under pressures. At $P=2\text{ GPa}$, the resistivity begins to *increase* with decreasing temperature below 10 K . This resistivity upturn is enhanced at higher pressures. Apparently, the pressure effect resembles that of the further K doping (see the above data of $x=0.26$). The result contrasts with the pressure-induced metallization in the parent compound BaMn_2As_2 .²²

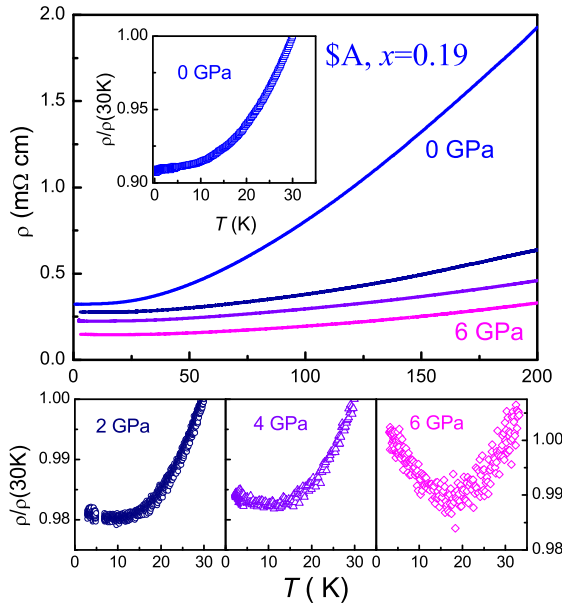


FIG. 3: (Color online) Temperature dependence of resistivity for $\text{Ba}_{0.81}\text{K}_{0.19}\text{Mn}_2\text{As}_2$ under high pressures.

We note that the $\rho(T)$ data of $x=0.05$ sample can be fitted by a power law $\rho = \rho_0 + AT^n$ with $n=2$ in a wide temperature range.²¹ However, the present heavily-doped samples have a change in the power exponent below 50 K (see the upper panel of Fig. 4), which is associated with a weak ferromagnetic transition below. The change in n from ~ 1.5 to ~ 2.5 can be explicitly seen in the series of plots with T^n as the horizontal axes. The transition temperature tends to increase with increasing K-content or pressure.

C. Magnetization

Figure 5 shows the magnetic susceptibility (χ) of the $\text{Ba}_{1-x}\text{K}_x\text{Fe}_2\text{As}_2$ single crystals. A remarkable magnetic anisotropy can be seen from the difference in $\chi_{ab}(T)$ and $\chi_c(T)$. The anisotropic ratio χ_{ab}/χ_c is over 10 below 100 K (see the inset of figure 6), indicating the easy magnetization along the ab -plane. The inset of Fig. 5 shows the $\chi_c(T)$ data separately. The $\chi_c(T)$ data of both samples have a positive temperature coefficient at high temperatures (the low-temperature upturn seems to be related to the weak ferromagnetic transition to be discussed below). This phenomenon is similar to that of the lightly K-doped sample reported previously,²¹ which still has a G -type AFM ground state with the Mn-moment along the c -axis. The $\chi_c(T)$ behavior for $x=0.19$ and $x=0.26$ reflects that the Mn local moments, oriented along the c -axis, are antiferromagnetically ordered above room temperature. If so, $\chi_{ab}(T)$ should be almost temperature-independent, as it is for the parent compound,²¹ because the applied field is perpendicular to the ordered moments.

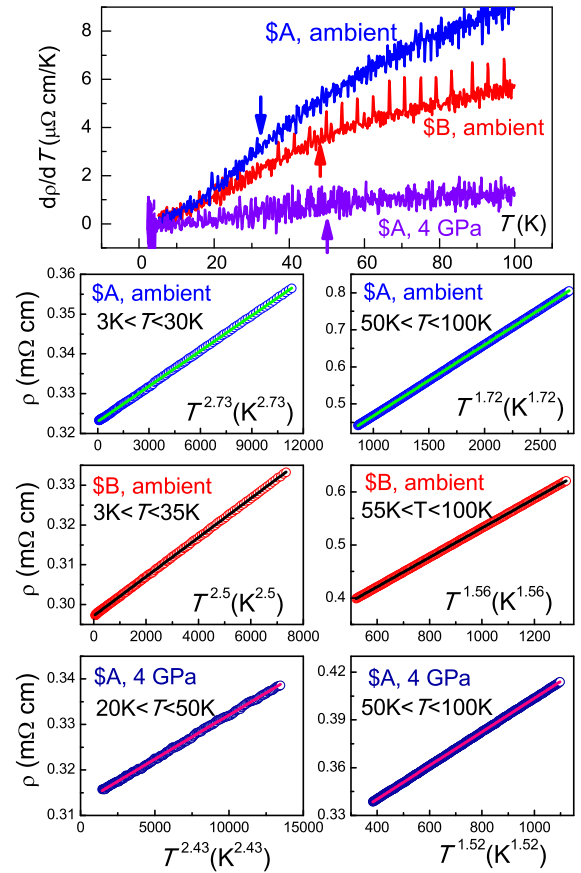


FIG. 4: (Color online) Upper panel: derivative of resistivity in $\text{Ba}_{1-x}\text{K}_x\text{Mn}_2\text{As}_2$ ($x=0.19$ for \$A and $x=0.26$ for \$B) single crystals. Other panels: plots of resistivity versus T^n , indicating a change in the power exponent below ~ 50 K.

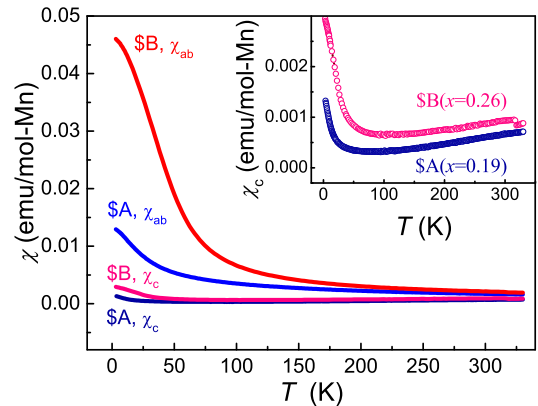


FIG. 5: (Color online) Temperature dependence of anisotropic magnetic susceptibility for $\text{Ba}_{1-x}\text{K}_x\text{Mn}_2\text{As}_2$ single crystals. The inset displays a magnified view for $\chi_c(T)$ ($H||c$). The small sudden increase in χ of the sample of $x=0.26$ at 317 K is due to the presence of tiny amount ($\sim 0.01\%$) of ferromagnetic MnAs impurity²⁷.

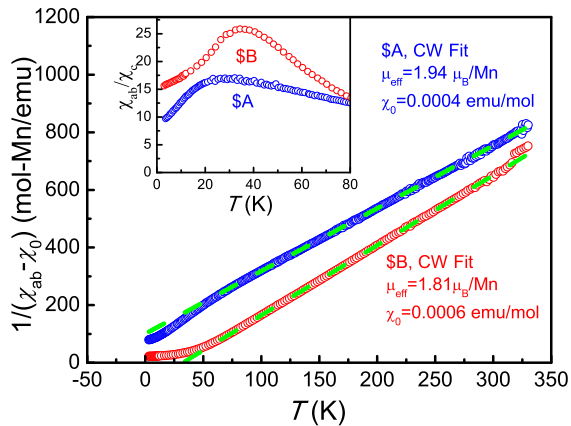


FIG. 6: (Color online) The reciprocal of the temperature-dependent in-plane magnetic susceptibility, showing Curie-Weiss behavior in $\text{Ba}_{1-x}\text{K}_x\text{Mn}_2\text{As}_2$ samples. The inset plots the anisotropy ratio $\chi_{ab}(T)/\chi_c(T)$.

However, the high-temperature $\chi_{ab}(T)$ data basically obeys Curie-Weiss law, as shown in Fig. 6. One has to ascribe this anomalous $\chi_{ab}(T)$ to the hole doping. This reminds us of the Curie-Weiss metallic state in Na_xCoO_2 ,²⁸ where a giant thermopower was rendered.^{29,30} By fitting the $\chi_{ab}(T)$ data with an extended Curie-Weiss formula, $\chi(T) = \chi_0 + C/(T - \theta)$, we obtained the effective moment of $1.81\mu_B/\text{Mn}$ ($1.94\mu_B/\text{Mn}$) for $x=0.26$ ($x=0.19$), equivalent to a local spin-1/2 paramagnet. The θ value for $x=0.26$ is 32 K and -47 K for $x=0.19$. This result suggests a magnetic exchange crossover from antiferromagnetic to ferromagnetic, via tuning the potassium doping level.

When $T < 50$ K where the ratio $\chi_{ab}(T)/\chi_c(T)$ shows a peak, χ_{ab} increases rapidly, or $1/\chi_{ab}$ has a positive curvature for both samples, especially for $x=0.26$. This suggests a ferromagnetic component, which is confirmed by the $M_{ab} - H$ plot showing in Fig. 7. At the temperatures above 55 K, the magnetization increases linearly with the applied field. At low temperatures, however, the $M_{ab} - H$ data show a jump in magnetization. The saturated magnetization M_{sat} is $0.02 \mu_B/\text{Mn}$ and $0.077 \mu_B/\text{Mn}$ for $x=0.19$ and $x=0.26$, respectively. A magnetic hysteresis in the $M_{ab} - H$ loop is clearly seen for $x=0.26$, further confirming the intrinsic weak ferromagnetism. Above 0.05 T, the isothermal magnetization increases almost linearly and very much slowly. Considered the large Mn local moment which is antiferromagnetically ordered above room temperature,²¹ this $M_{ab}(H)$ behavior suggests dominant local-moment antiferromagnetism. The $M_c - H$ curve at 3 K for the $x=0.26$ crystal shows tiny saturated magnetization of $0.005 \mu_B/\text{Mn}$ (not shown here). So, the spontaneous ferromagnetic moment is basically along the basal planes. The absence of magnetic hysteresis and smaller saturated magnetization for the sample of $x=0.19$ suggest that it is on the verge of the emergent ferromagnetism.

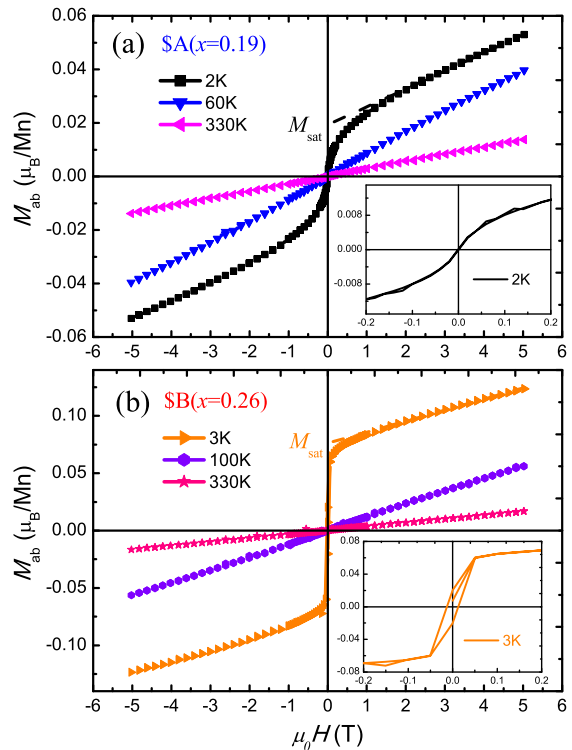


FIG. 7: (Color online) Isothermal $M_{ab} - H$ data at different temperatures for samples A ($x=0.19$) and B ($x=0.26$). The insets show the enlarged $M_{ab} - H$ data at 2 K and 3 K.

D. Electronic Structure Calculation

In order to understand the K-doping effect in BaMn_2As_2 , we employed first-principles electronic structure calculations. The band structure of the undoped compound in Fig. 8(a) shows an indirect band gap of 0.11 eV, which is consistent with the results of above resistivity measurement and the previous calculations.^{14,21} The projected DOS indicates strong spin-dependent hybridization between Mn-3d and As-4p states, which explains the reduced moment of $3.8 \mu_B/\text{Mn}$. The As-4p DOS can be better accounted for the difference between the total DOS and the Mn 3d projection.⁸ Thus we conclude that, compared with the conduction bands, the valence bands have much more As-4p weight. In this regard, the parent compound can be considered as a charge-transfer insulator with strong Hund's rule coupling.

By using supercell approximation, we were able to calculate the electronic structure of $\text{Ba}_{0.75}\text{K}_{0.25}\text{Mn}_2\text{As}_2$, which is very close to the case of Sample B. As shown in Fig. 8(b), though much more band dispersions appear near the Fermi energy due to the use of supercell, the main features are maintained (e.g., a bandgap of ~ 0.1 eV still appears above E_F), except that the Fermi level is shifted down by about 0.2 eV owing to the hole doping. The shift of E_F makes multiple hole-like Fermi surfaces, which account for the metallic behavior in BKMA. Be-

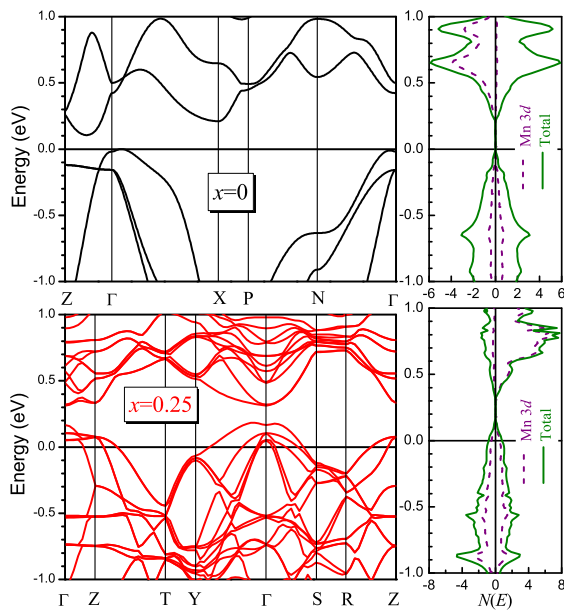


FIG. 8: (Color online) Band structures of BaMn_2As_2 (upper panel) and $\text{Ba}_{0.75}\text{K}_{0.25}\text{Mn}_2\text{As}_2$ (lower panel). The right panels show the corresponding total and projected (Mn $3d$) density of states (DOS). The negative DOS refer to the opposite spin.

cause As- $4p$ holes usually have much higher mobility than the Mn- $3d$ holes do, the metallic conductivity should be mainly contributed by the As- $4p$ holes. Therefore, the anomalous resistivity minimum under pressures may be explained in terms of pressure-enhanced Kondo-like magnetic scattering of the conduction holes.

Except for the rigid band scenario, the main modification in the electronic structure of BKMA is that the As- $4p$ weight at E_F is reduced, suggesting that the K doping weakens the $p-d$ hybridizations. Consistent with the reduced hybridization, the calculated AFM local moment is significantly increased to $4.9 \mu_B/\text{Mn}$, close to the value of a free Mn^{2+} ion, and consistent with the previous neutron diffraction result ($4.2 \mu_B/\text{Mn}$ for $x=0.05$).²¹

Now let us briefly discuss the possible physics of the anomalous properties in BKMA. The weak ferromagnetism should be either local or itinerant. In the local case, the ferromagnetism is easily accounted for by the canting (toward the basal planes) of the Mn local moment. The mechanism could be like the double exchanges

in manganites.³¹ Note that the saturation magnetization is much lower than the Mn local moment, therefore, such spin canting would be very slight. The second is an itinerant ferromagnetism scenario, in which the doped As $4p$ holes and/or Mn $3d$ holes are simply spin-polarized. In this case, the saturation magnetization should be comparable with the doping level per Mn ($x/2$), which basically agrees with the experimental saturation moment. The Curie-Weiss-like in-plane magnetic susceptibility resembles the behavior of Na_xCoO_2 ($x \sim 0.7$), as we pointed out above, suggests correlated metallicity in the present system. As for the resistivity minimum at high pressures, one has to consider the interactions between conduction holes and the local moments, but we have not arrived a definite picture so far. In a word, the interplay between itinerant $4p$ holes and local $3d$ moments seems to be very crucial. Future studies are called for to clarify all the novel properties shown in $\text{Ba}_{1-x}\text{K}_x\text{Mn}_2\text{As}_2$ system.

IV. CONCLUDING REMARKS

In summary, we have successfully synthesized heavily-doped $\text{Ba}_{1-x}\text{K}_x\text{Mn}_2\text{As}_2$ ($x=0.19$ and 0.26) single crystals which showed good homogeneity and crystallinity. By measuring the resistivity and magnetization, we confirmed metallization by a hole doping with potassium in BaMn_2As_2 . Several anomalous properties in the metallic state were demonstrated. First, a weak ferromagnetic transition at ~ 50 K was discovered. Second, the low-temperature resistivity behaves a Kondo-like minimum upon applying high pressures. Third, the in-plane magnetic susceptibility shows Curie-Weiss behavior, though being in an AFM state. Our electronic structure calculations indicate that the As $4p$ holes are most likely responsible for the metallic conduction. Therefore, these novel metallic behaviors reflect the interplay between itinerant $4p$ holes and local $3d$ moments in $\text{Ba}_{1-x}\text{K}_x\text{Mn}_2\text{As}_2$ system.

Acknowledgments

This work is supported by the NSF of China (nos 11190023, 90922002 and 10934005) and the National Basic Research Program of China (nos 2010CB923003).

* corresponding author: ghcao@zju.edu.cn

¹ Y. Kamihara, T. Watanabe, M. Hirano, and H. Hosono, *J. Am. Chem. Soc.* **130**, 3296 (2008).

² For a review, see: D. C. Johnston, *Adv. Phys.* **59**, 803 (2010).

³ M. Imada, A. Fujimori, and Y. Tokura, *Rev. Mod. Phys.* **70**, 1039 (1998).

⁴ Y. Shiomi, S. Ishiwata, Y. Taguchi, and Y. Tokura, *Phys.*

Rev. B **84**, 054519 (2011).

⁵ Yunlei Sun, Jinke Bao, Yongkang Luo, Chunmu Feng, Zhuan Xu, and Guanghan Cao, *EPL* **98**, 17009 (2012).

⁶ Q. Huang, Y. Qiu, Wei Bao, M. A. Green, J. W. Lynn, Y. C. Gasparovic, T. Wu, G. Wu, and X. H. Chen, *Phys. Rev. Lett.* **101**, 257003 (2008).

⁷ M. Rotter, M. Tegel, and D. Johrendt, *Phys. Rev. Lett.* **101**, 107006 (2008).

- ⁸ D. J. Singh, A. S. Sefat, M. A. McGuire, B. C. Sales, D. Mandrus, L. H. VanBebber, and V. Keppens, *Phys. Rev. B* **79**, 094429 (2009).
- ⁹ A. S. Sefat, D. J. Singh, R. Jin, M. A. McGuire, B. C. Sales, and D. Mandrus, *Phys. Rev. B* **79**, 024512 (2009).
- ¹⁰ F. Ronning, N. Kurita, E. D. Bauer, B. L. Scott, T. Park, T. Klimczuk, R. Movshovich, and J. D. Thompson, *J. Phys. Condens. Matter* **20**, 342203 (2008); N. Kurita, F. Ronning, Y. Tokiwa, E. D. Bauer, A. Subedi, D. J. Singh, J. D. Thompson, and R. Movshovich, *Phys. Rev. Lett.* **102**, 147004 (2009).
- ¹¹ E. Brechtel, G. Cordier, and H. Schaefer, *Z. Naturforsch.* **33b**, 820 (1978).
- ¹² Y. Singh, A. Ellern, and D. C. Johnston, *Phys. Rev. B* **79**, 094519 (2009).
- ¹³ Y. Singh, M. A. Green, Q. Huang, A. Kreyssig, R. J. McQueeney, D. C. Johnston, and A. I. Goldman, *Phys. Rev. B* **80**, 100403(R) (2009).
- ¹⁴ J. An, A. S. Sefat, D. J. Singh, and M.-H. Du, *Phys. Rev. B* **79**, 075120 (2009).
- ¹⁵ D. C. Johnston, R. J. McQueeney, B. Lake, A. Honecker, M. E. Zhitomirsky, R. Nath, Y. Furukawa, V. P. Antropov, and Y. Singh, *Phys. Rev. B* **84**, 094445 (2011).
- ¹⁶ A. S. Sefat, R. Jin, M. A. McGuire, B. C. Sales, D. J. Singh, and D. Mandrus, *Phys. Rev. Lett.* **101**, 117004 (2008).
- ¹⁷ L. J. Li, Y. K. Luo, Q. B. Wang, H. Chen, Z. Ren, Q. Tao, Y. K. Li, X. Lin, M. He, Z. W. Zhu, G. H. Cao, and Z. A. Xu, *New J. Phys.* **11**, 025008 (2009).
- ¹⁸ S. Jiang, H. Xing, G. Xuan, C. Z. Ren, C. Feng, J. Dai, Z. Xu, and G. Cao, *J. Phys. Condens. Matter* **21**, 382203 (2009).
- ¹⁹ M. S. Torikachvili, S. L. Budko, N. Ni, and P. C. Canfield, *Phys. Rev. Lett.* **101**, 057006 (2008); T. Park, E. Park, H. Lee, T. Klimczuk, E. D. Bauer, F. Ronning, and J. D. Thompson, *J. Phys.: Condens. Matter* **20**, 322204 (2008).
- ²⁰ A. Pandey, V. K. Anand, and D. C. Johnston, *Phys. Rev. B* **84**, 014405 (2009).
- ²¹ A. Pandey, R. S. Dhaka, J. Lamsal, Y. Lee, V. K. Anand, A. Kreyssig, T. W. Heitmann, R. J. McQueeney, A. I. Goldman, B. N. Harmon, A. Kaminski, and D. C. Johnston, *Phys. Rev. Lett.* **108**, 087005 (2012).
- ²² A. T. Satya, Awadhesh Mani, A. Arulraj, N. V. Chandra Shekar, K. Vinod, C. S. Sundar, and A. Bharathi, *Phys. Rev. B* **84**, 180515(R) (2011).
- ²³ Crystal growth of K-doped BaMn₂As₂ and observation of weak-ferromagnetic metallic state were reported at the 2011 Fall Meeting of the Chinese Physical Society (September 2011, Hangzhou, China).
- ²⁴ N. Mori, H. Takahashi, and N. Takeshita, *High Press. Res.* **24**, 225 (2004).
- ²⁵ M. Segall, P. Lindan, M. Probert, C. Pickard, P. Hasnip, S. Clark, and M. Payne, *J. Phys.: Condens. Matter* **14**, 2717 (2002).
- ²⁶ N. F. Mott, *Metal-Insulator Transitions* (Taylor and Francis, London, 1990).
- ²⁷ C. P. Bean and D. S. Rodnell, *Phys. Rev.* **126**, 104 (1962).
- ²⁸ M. L. Foo, Y. Y. Wang, S. Watauchi, H. W. Zandbergen, T. He, R. J. Cava, N. P. Ong, *Phys. Rev. Lett.* **92**, 247001 (2004).
- ²⁹ I. Terasaki, Y. Sasago, and K. Uchinokura, *Phys. Rev. B* **56**, 12685(R) (1997).
- ³⁰ Unfortunately, our crystals are too small to make a reliable thermopower measurement. However, La_{0.9}Sr_{0.1}MnAsO indeed shows a very large thermopower at room temperature (Ref. 5).
- ³¹ C. Zener, *Phys. Rev.* **82**, 403 (1951); P. W. Anderson, H. Hasegawa, *Phys. Rev.* **100**, 675 (1955); P. G. de Gennes, *Phys. Rev.* **118**, 141 (1960).